ACS OMEGA

Article

Cite This: ACS Omega 2018, 3, 6794−6803

Physics behind the Barrier to Internal Rotation of an Acetyl Chloride Molecule: A Combined Approach from Density Functional Theory, Car−Parrinello Molecular Dynamics, and Time-Resolved Wavelet Transform Theory

Bipan Dutta,[†] Biplab Bhattacharjee,[‡] and Joydeep Chowdhury*[,§]

[†]Department of Physics, Sammilani Mahavidyalaya, E. M. Bypass, Baghajatin Station, Kolkata 700094, India

[‡]Department of Chemistry and [§]Department of Physics, Jadavpur University, 88, Raja S. C. Mallick Road, Kolkata 700032, India

Supporting Information

ABSTRACT: The physics behind the barriers to internal rotation of acetyl chloride (AC) molecule has been reported. The AC molecule closely resembles the molecular structure of acetaldehyde; the only subtle difference is the presence of a heavy chlorine atom in place of the hydrogen atom of the aldehyde group for the latter. This paper aims to study the effect of substitution of the heavy chlorine atom on the barrier energetics of the AC molecule. The reason behind the barrier for the AC molecule has been estimated for the first time from the unified approach using barrier energetics, natural bond orbital, nuclear virial, and relaxation analyses using density functional theory, Car−Parrinello molecular dynamics, and wavelet transform theory. Complete analyses reveal the concomitant relaxations of both the in-plane $C_{methyl}-C_1$ and $C_{methyl}-H_4$ bonds toward understanding the origin of the barrier due to internal rotation for the AC molecule. The large negative value of "V_6" further suggests that both the abovementioned degrees of freedom are coupled with the $-CH_3$ torsional vibration of the molecule. The coupling matrix (H_{12}) element has also been estimated. Time-resolved band stretching frequencies of $C_{methyl}-C_1$ and C_1-Cl_3 bonds of the AC molecule, as obtained from wavelet transformation analysis, primarily preclude the possibility of coupling between the C_1-Cl_3 bond and the torsional motion associated with the methyl group of the molecule.

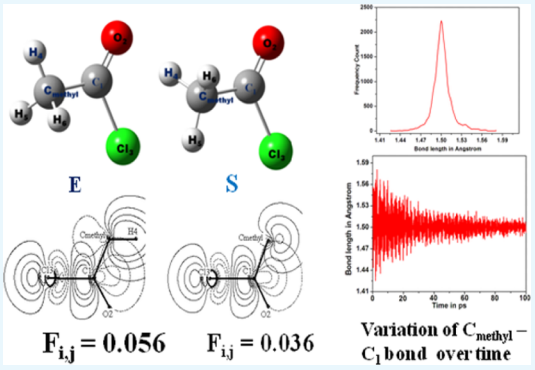

1. INTRODUCTION

Molecular conformations play important roles in the world of macromolecules, whose structure−function relationship contributes significantly toward understanding the basic physics and chemistry behind the functioning of complex biological systems.[1] A molecule, in principle, can undergo conformational changes by internal rotation, ideally about the concerned single bond/bonds. The text book example of such internal rotation is observed in ethane, as it takes the stereoisomeric eclipsed and staggered conformations with the change in the specific dihedral angle. However, the real existence of this type of stereoisomeric conformers apparently seems to depend explicitly on the torsional angle τ.[2] The barrier energy or height that separates two distinct conformations is fundamentally the effect of hindered rotation, stemming toward the concept of barrier potential. Interestingly, the quantum mechanical nature of hindered rotation was first identified by Nielsen in 1932.[3] The theoretical results from his group provide the initial plunge behind the phenomenal paper by Pitzer[4] on the internal rotation of the ethane molecule. Since then, the estimations of barrier heights have been extended to other molecules involving three- or even 6-fold barriers.[5] The results were primarily collected with the aid of microwave spectroscopy from the splitting of rotational transitions into doublet, triplet, and quadruplet structures because of the internal rotation of the rotor group. Other experimental approaches to find barrier heights of conformeric molecules are from Raman and far-infrared spectroscopic investigations. For both these techniques, the torsional fundamental and overtone vibrational signatures provide the means of such estimations.[6] Moreover, fluorescence, supersonic jet-cooled, and the analyses of hot bands from UV−vis electronic spectroscopy also provide wealth of information toward the estimations of barriers heights.[7] Intriguingly, in the late fifties and early sixties of the twentieth century, Wilson et al. implicitly linked the origin of barrier heights with the electronic structures of molecules.[8] Understanding the origin of rotational barriers from the electronic structures of molecules was further facilitated by the advancement of quantum chemical calculations.[9] However, increasing availabilities of faster computations allow us to undergo in depth quantum mechanical studies to elucidate the unexplored physics behind the origin of

Received: February 22, 2018
Accepted: May 18, 2018
Published: June 22, 2018

DOI: 10.1021/acsomega.8b00316
ACS Omega 2018, 3, 6794−6803

rotational barriers. Goodman and his research group had accomplished remarkable breakthrough in this area of research, where the nature of barrier forces and the role of lone pairs toward understanding the internal rotational barriers of molecules were explicitly studied for single or double rotor systems.[10] Recently, our research group has estimated the origins of 3-fold rotational and conformational barriers of ethyl propionate and isobutyl cyanide molecules containing two methyl groups.[11] The results show that the involvement of both the bond length and skeletal angle relaxations together play a prominent role in controlling the estimated barrier heights of such molecules. However, the basic question still remains: how to integrate the experimental results with the theoretical understanding behind the genesis of internal rotational barriers of conformeric molecules. The obvious way of fitting the experimental transitions on a one-dimensional potential energy curve (PEC) as a function of the torsional angle (τ) is elusive, considering its multidimensional nature per se. The theoretical calculations supplement the experimental observations with the inclusion of nontorsional degrees of freedom of the molecules and provide a complete panorama toward closer understanding of the origin of internal rotational barriers of the molecules. The self-consistent field (SCF) calculations further obey the variational principle toward the astute guesses of the minimum energy configurations of the molecules.

As part of a series, Guo and Goodman reported the nature of barrier forces for the acetaldehyde molecule and highlighted the importance of coupling between the methyl torsional and out-of-plane aldehyde hydrogen wagging motions toward overall understanding of its barrier origin.[12] Considering the above-mentioned results in mind, here, we report the origin of rotational barriers of acetyl chloride (AC) molecules, which have a very close resemblance with those of acetaldehyde. Unlike acetaldehyde, in AC, the hydrogen of the aldehyde group is replaced by the heavy chlorine (Cl) atom, and we aim to study the effect of substitution on the barrier energetic of the molecule. Substitution of the heavy chlorine atom in place of hydrogen is expected to restrict the wagging motion of the C−Cl bond and primarily preclude its possibility of coupling with the torsional motion of the methyl group of the molecule. This paper is primarily focused to unveil the origin of the internal rotational barrier of the AC molecule for the first time from the unified approach using barrier energetic, natural bond orbital, nuclear virial (NV), and relaxation analyses. The Raman vibrational signatures and the corresponding dynamic infrared (IR) spectrum of the molecule have been simulated from density functional theory (DFT) calculations and from Car−Parrinello molecular dynamics (CPMD), respectively. The barrier height of this molecule is estimated from microwave and Raman spectroscopic studies and is reported in the literature.[13,14] The available experimental results encourage us to elicit the origin behind the barrier to the internal rotation for the AC molecule from theoretical considerations.

2. THEORETICAL CALCULATIONS

All theoretical calculations were carried out using Gaussion-09 suit of the program mentioned in ref 15. Optimizations and vibrational frequencies of the different rotameric forms of the AC molecule were computed from Møller−Plesset perturbation by the MP2/6-21G(d) level of theory. To understand the physics behind the methyl rotational barrier of the AC molecule, the virial theorem[16] has been satisfied using different basis sets ranging from 3-21G to aug-cc-pVTZ in the ab initio and in DFT calculations with the B3LYP functional. However, the theorem is best satisfied at MP2/6-31G(d) and B3LYP/6-31G(d,p) levels of theory with $\Delta T + \Delta E$ equals to 0.14 and 0.02 kcal/mol, respectively. Thus, the origin of the methyl rotational barrier of the AC molecule was carried out from DFT calculations using the B3LYP functional and the 6-31G(d,p) basis set in addition to the ab initio MP2/6-21G(d) level of theories. In this connection, it may be firmly mentioned that reasonable barrier heights are reported to be reproducible for many molecules even by HF calculations using a modest 6-31G (d,p) basis set.[11a,12]

Ab initio molecular dynamics (MD) simulations have been carried out using the CPMD program[17] with the pre-optimized structure of the AC molecule. The CPMD approach is based on the electronic optimization scheme, where a fictitious electronic mass is assigned to the propagating orbitals of the electrons. The two component quantum/classical problems are mapped onto a two-component purely classical problem, with two separate energy scales at the expense of losing the explicit time-dependence of the quantum subsystem dynamics.[18] The structure of the AC molecule is placed at the center of a simple cubic cell of dimension 10.0 × 10.0 × 10.0 Å^3. The NVT ensemble has been chosen to execute the simulation at room temperature over an equilibrium time of 100 ps. The time step was set to 4.0 au that corresponds to ∼0.096 fs. The temperature of the ensemble was controlled through the Nose−Hoover thermostat.[19] An electronic fictitious mass parameter of 500 a. u. has been used in the simulation run. The gradient-corrected Perdew, Burke, and Ernzerhof (PBE) functional[20] has been utilized to model the electronic exchange and correlation factors. Core electrons were treated with pseudo potentials of Troullier and Martins,[21] while valance electrons were represented by the plane-wave basis set truncated at an extended energy cutoff of 80 Ry.

The vibrational signatures of the molecule are obtained from time-dependent molecular dynamics trajectories, with the aid of Fourier transformations. From CPMD trajectories, the stretching distances of atoms as a function of time, associated with the vibrational modes of the molecule, are extracted. The vibrational density of states (VDOS) of the respective normal modes is then obtained from Fourier transformation. Wavelet transform is then employed to estimate the frequency−time plot for individual normal modes of vibration of the molecule.

The algorithm adopted to compute wavelet transform $W_n(s)$ in the Fourier space is expressed as[22]

$$W_n(s) = \sum_{k=1}^{N-1} \hat{F}_k \hat{\psi}(s\omega_k)\, e^{i\omega_k n\delta t} \quad (1)$$

where ω_k is the angular frequency for the kth normal mode and $\hat{F}_k$ and $\hat{\psi}$ are the Fourier transformations of the time series F_n and the mother wavelet $\psi(t)$, respectively. The mother wavelet $\psi(t)$ is represented as

$$\psi(t) = \pi^{-1/4}\, e^{i\omega_0 t - t^2/2\sigma^2} \quad (2)$$

where the parameters ω_0 and σ are set as reported elsewhere.[23] The functional form of eq 2 is given by the Morlet function, and Kirby and Swain[24] proved that it reproduces the Fourier power spectrum.

The IR spectrum of the AC molecule has been estimated from "on the fly" dynamics. The dynamic IR spectrum of the AC molecule has been simulated from Fourier transform of the dipole moment autocorrelation function (DMAF). The de-

DOI: 10.1021/acsomega.8b00316
ACS Omega 2018, 3, 6794−6803

tailed description of DMAF is given in the Supporting Information.

3. RESULTS AND DISCUSSION

The optimized structures of the AC molecule are shown in Figure 1. The molecule exists in eclipsed (E) and in staggered

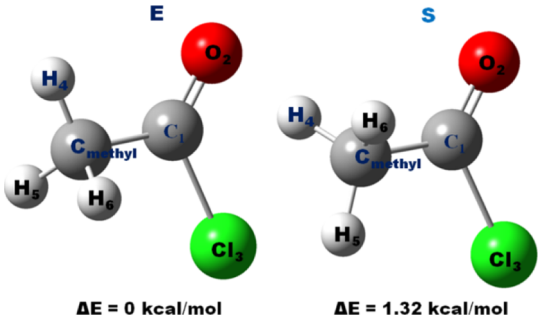

Figure 1. Optimized molecular structures and respective SCF energies of the "E" and "S" forms of the AC molecule as obtained from the MP2/6-21G(d) level of theory.

(S) conformations. The simulated Raman and IR spectra, as obtained from the MP2 level of theory, are shown in Figure 2a,b, respectively. The differential Raman scattering cross-section ($d\sigma/d\Omega$) values have been estimated from the scattering activities using the relationship[25]

$$I_{\text{Raman}} = \left(\frac{d\sigma}{d\Omega}\right)_i = \frac{(2\pi)^4}{45}\frac{h}{8\pi^2 c\omega_i}\frac{(\omega_0 - \omega)^4}{1 - \exp(-hc\omega_i\beta)}S_i \quad (3)$$

where $\beta = 1/K_B T$, $S_i = 45\left(\frac{d\alpha}{dQ_i}\right)^2 + 7\left(\frac{d\gamma}{dQ_i}\right)^2$ represents the Raman scattering factor (in Å^4/amu) of the molecule excited with "ith" wavelength expressed in nanometers. The expression S_i is calculated at the equilibrium geometry, and it is the expression of derivatives in terms of static isotropic (α) and anisotropic (γ) polarizabilities.

The spectra, as shown in Figure 2a,b, are marked by the appearance of well-resolved Raman and IR bands in the entire spectral window ranging from 0 to 3000 cm^{-1}. Insets of Figure 2a,b further mark the presence of low-frequency vibrational signatures centered at ∼164 and 163 cm^{-1}, respectively. This band is ascribed to the torsional vibration stemming from the methyl—CH_3 top of the AC molecule. The result is in accordance with the experimental observation as reported by Durig et al. from the Raman spectrum of the molecule reported in the solid state.[13]

The simulated dynamic IR spectrum of the AC molecule has been also estimated from "on the fly" CPMD simulation studies. The spectrum is shown in Figure 2c. The theoretically simulated IR spectrum, as obtained from CPMD calculation, is also marked by the presence of a broad hump centered at ∼149 cm^{-1} in the low wavenumber region. This band, albeit weak, has been identified with the torsional vibration of the molecule centered at 166, 164, and 163 cm^{-1} in the experimental and theoretically simulated Raman and IR spectra, respectively, as obtained from the MP2 calculations. The IR spectrum, as obtained from CPMD simulations, however, appears to differ especially in the 1250−2000 cm^{-1} with the corresponding spectrum as estimated from the MP2 level of theory. The reason for this difference may be partly owing to the

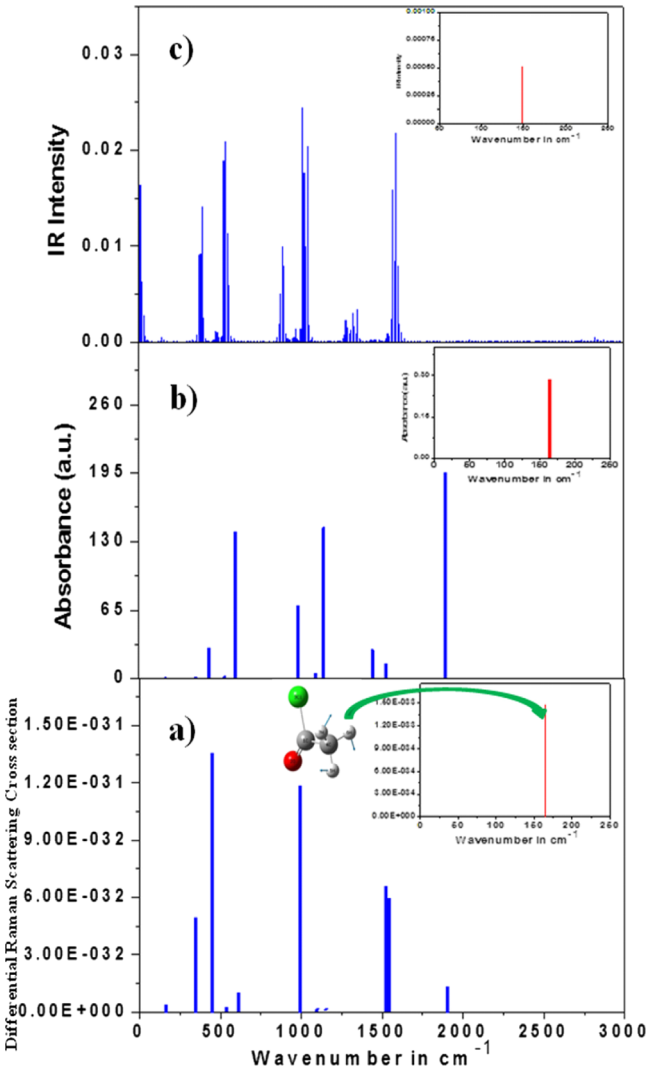

Figure 2. Simulated: gas-phase (a) Raman spectrum, (b) IR spectrum, and (c) dynamic IR spectrum of the AC molecule using MP2/6-21G(d) and CPMD simulation studies.

anharmonicity of the vibrations. However, the other probable explanation may be the effect of finite fictitious electronic mass parameters that is considered in the CPMD simulation run.[26] The effect of finite fictitious electron mass makes the moving nuclei effectively heavier. The velocity or the DMAF averaged over a period of time and the corresponding dynamic IR spectrum of the molecule are highly mass-dependent quantities. The effect of the finite fictitious electron mass thus has a direct impact on the vibrational wavenumbers as estimated from CPMD simulations in comparison with that calculated from the MP2 level of theory. Hence, the anharmonicity of the vibrations together with the effect of finite fictitious electron mass (making the moving nuclei heavier) effectively make the IR spectra calculated at MP2 and CPMD level of theories look so different.

The shape of the PEC associated with the methyl rotation of the AC molecule has been estimated as a function of $O_2-C_1-C_{methyl}-C_4$ torsional angle (τ). The PEC is shown in Figure S1. The bottom and the top of the barrier in the PEC correspond to the "E" and "S" conformers of the AC molecule, respectively. The optimized structural parameters of "E" and "S" forms of the AC molecule, as obtained from ab initio, DFT, and CPMD

DOI: 10.1021/acsomega.8b00316
ACS Omega 2018, 3, 6794−6803

calculations, are shown in Table S1. The central carbon C_{methyl} atom of the $-CH_3$ group in the AC molecule is ~sp^3-hybridized with the relevant bond angle ~110.61°, 110.55°, and 109.98° as obtained from MP2/6-21G(d), B3LYP/6-31G(d,p), and CPMD level of theories, respectively. The Cartesian displacement of the abovementioned vibrational signature is also shown in Figure 2a. The torsional frequency of the methyl—CH_3 group is utilized to estimate the 3-fold (V_3) rotational barrier of the molecule by using the relation we used before[10a]

$$V_3 = \frac{8}{9}\pi^2\nu^2 I_r \tag{4}$$

where ν is the torsional frequency and I_r is the reduced moment of inertia of the methyl ($-CH_3$) group with respect to the center of gravity of the AC molecule. The 3-fold barrier (V_3) to internal rotation for the $-CH_3$ group of the AC molecule is estimated to be ~1.32 and 1.31 kcal/mol using MP2/6-21G(d) and B3LYP/6-31G(d,p) level of theories, respectively.

The classical approach to envisage the rotational barriers of molecules containing a single rotor is the obvious expansion of the hindered potential function $V(\tau)$ in the Fourier series for various torsional angles (τ). It is represented as

$$V(\tau) = \frac{1}{2}\sum_n V_n(1 - \cos n\tau) \tag{5}$$

The methyl group of the AC molecule has 3-fold symmetry, and the equivalent configurations reproduce themselves through permutations of the three hydrogen atoms. Thus, only the odd components survive in the abovementioned expression 5, which takes the following form.

$$V(\tau) = \frac{1}{2}V_3(1 - \cos 3\tau) + \frac{1}{2}V_6(1 - \cos 6\tau) + \frac{1}{2}V_9(1 - \cos 9\tau) + \ldots \tag{6}$$

The term "V_3" determines the height of the barrier, while its shape is intimately linked with the term "V_6". The shape of the barrier "V_6" is related with the dynamics and splitting of energy levels, as the response behavior to the torsional tunneling. The "V_6" term is much less than "V_3" and contributes even less than 3% of it. Because "V_9" carries no special physical significance and as $V_9 \ll V_3$, the abovementioned series is truncated up to "V_6".

Table S2 shows the values of V_i (i = 3, 6) for the internal rotation of the methyl—CH_3 of the AC molecule. It is seen from Table S2 that "V_3" as obtained from the fitting function (vide supra) is in close harmony with that estimated from torsional vibration of the Raman spectrum of the AC molecule.[13] The "V_6" value has been estimated to be −0.019 kcal/mol. The negative sign of "V_6" for the AC molecule is in accordance with that reported by Kudich et al.,[27] where the values of "V_6" had been predicted to vary between −10.5 and −11.4 cm^{-1}, depending upon the level of theories computed over different basis sets. In this connection, it is also worth to mention that for the acetaldehyde molecule, the sign of the corresponding "V_6" term is also negative[28] for fully relaxed optimizations, signifying strong coupling of methyl torsion with the out-of-plane γ ($C_{aldehyde}$−H) wagging motion of the molecule. However, in general, the negative sign of "V_6" affects the shape of the barrier; it deepens the potential well, narrows the barrier, and decreases the torsional energy levels of the rotor.

To understand the primary origin of the 3-fold (V_3) rotational barrier of the AC molecule, the effects of strain within the molecule have been estimated from the generalized virial theorem. The generalized virial theorem[29] provides a simple yet elegant route for understanding the origin behind the barriers.

Accordingly

$$T = -E + \sum_\alpha \vec{\chi}_\alpha \vec{F}_\alpha \tag{7}$$

where $\sum_\alpha \vec{\chi}_\alpha \vec{F}_\alpha$ is the NV and the summation signifies the sum over contribution of the nucleus α to the virial of force acting on the electrons. The position vector of the nucleus α is $\vec{\chi}_\alpha$, and $\vec{F}_\alpha = \vec{\nabla}_\alpha E$ is the net force acting on it.

The variations of NV for rigid rotation (RR) and for the skeletal relaxations alone or in combination as a function of torsion angle (τ) are shown separately in Figure 3a,b using

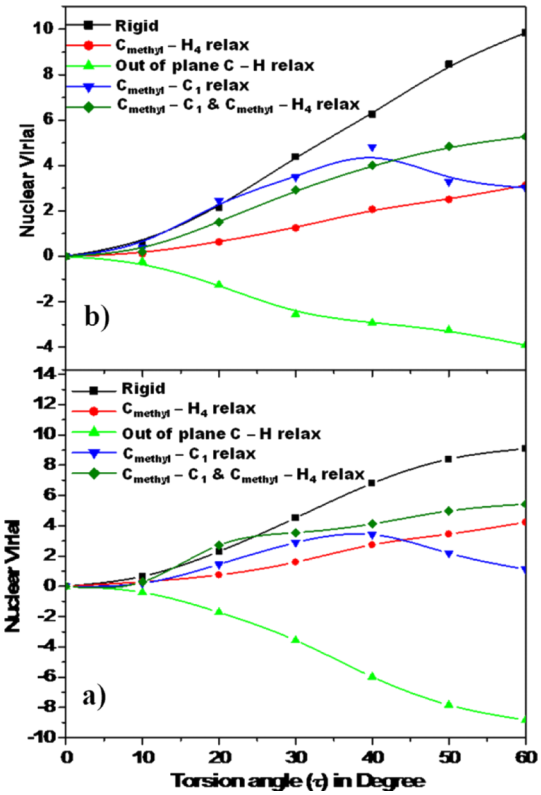

Figure 3. NVs for internal rotational barrier of the CH_3 group of the AC molecule using (a) B3LYP/6-31G(d,p) and (b) MP2/6-21G(d) level of theories.

DFT and ab initio levels of theories, respectively. Interestingly, both the levels of theory are almost reproducible and exhibit similar observations, as apparent from Figure 3a,b. From Figure 3 it is seen that, NV monotonically increases with τ on going from "E" to "S" in the case of RR for the $-CH_3$ group of the AC molecule. The increasing value of the NV, as the torsional angle τ proceeds toward 60°, may signify that the molecule is left in a strained metastable state in the "S" conformation. However, with the inclusion of the out-of -plane C_{methyl}−H skeletal flexing, the NV shows an antagonistic behavior with respect to RR. Interestingly, when C_{methyl}−C_1 is allowed to

DOI: 10.1021/acsomega.8b00316
ACS Omega 2018, 3, 6794−6803

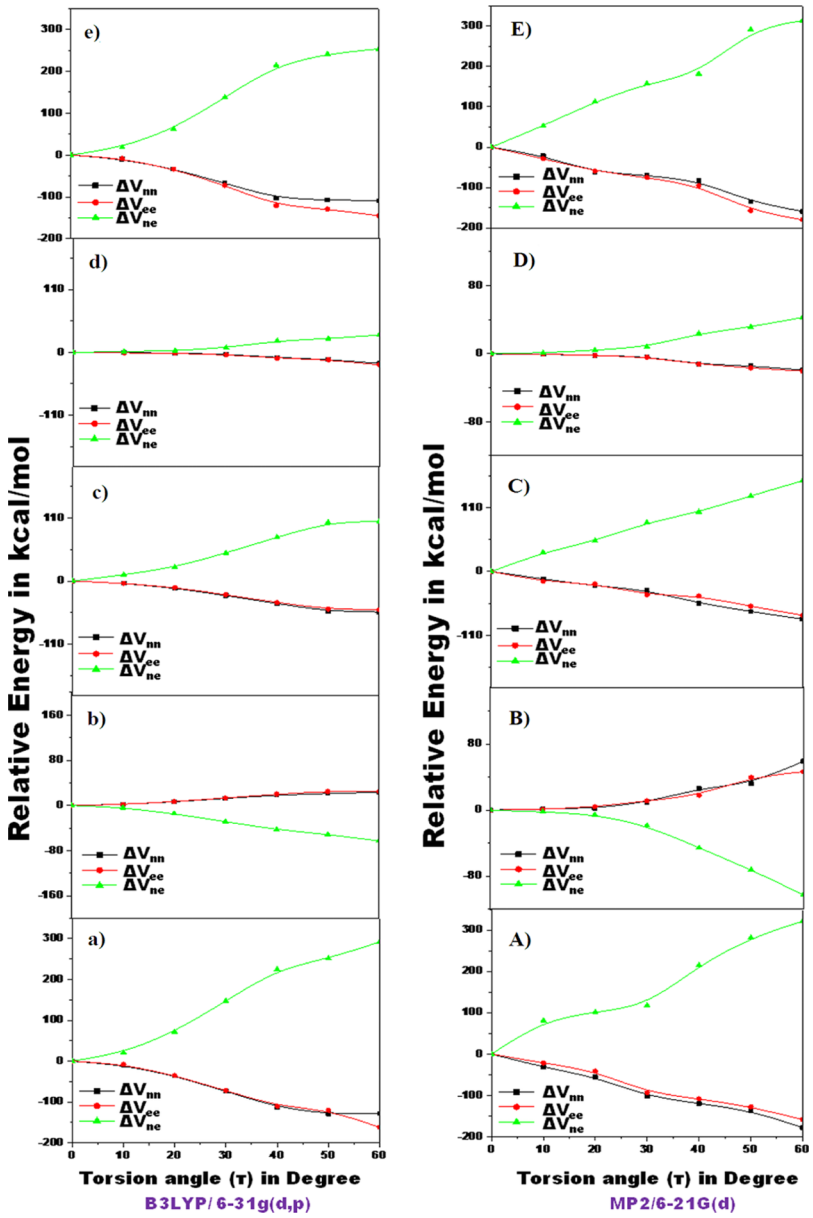

Figure 4. Rotational dependence of the ΔV_{nn}, ΔV_{ee}, and ΔV_{ne} of the (a,A) fully relaxed, (b,B) RR, (c,C) in-plane C_{methyl}–C_1 relax, (d,D) in-plane C_{methyl}–H_4 relax, and (e,E) in-plane C_{methyl}–C_1 and C_{methyl}–H_4 skeletal flexing of the AC molecule.

relax, NV initially increases with τ, maximizes near 40°, and decreases again as τ approaches toward "S" conformation. The NV, with the inclusion of in-plane C_{methyl}–H_4 skeletal flexing, again increases monotonically, similar to that observed for the RR of the molecule, albeit its magnitude is small in comparison to RR. However, when both the C_{methyl}–C_1 and in-plane C_{methyl}–H_4 flexing are allowed to relax, keeping other degrees of freedom for the frozen molecule, the variation of NVs as a function of τ closely resembles that for RR. These results indicate that the strain generated in going from E to S mainly arises from the combined effect of frozen C_{methyl}–C_1 and in-plane C_{methyl}–H_4 skeletal flexing of the AC molecule.

To identify specific importance of relaxations of the C_{methyl}–C_1 and C_{methyl}–H_4 bonds alone or in combination toward the stereoisomeric dispositions of "E" to "S" conformations of the AC molecule, the variations of Coulomb repulsion (ca. ΔV_{nn} and ΔV_{ee}) and nuclear–electron attraction (ca. ΔV_{ne}) as a function of the torsion angle (τ) have been considered. The variations are shown in Figure 4, as obtained from DFT and the ab initio level of theories. Similar to the estimation of NVs, the variations of potential energy differences for ΔV_{nn}, ΔV_{ee}, and ΔV_{ne} as a function of τ, as obtained from two different levels of theories are almost similar. For fully relaxed rotations, ΔV_{ne} is the dominant barrier forming the term, while ΔV_{nn} and ΔV_{ee} contribute toward the antibarrier energy [Figure 4a,A]. Interestingly, for RR, ΔV_{ne} turns out to the most prominent antibarrier-forming energy, while the energy profiles for ΔV_{nn} and ΔV_{ee} are almost superimposed and collectively contribute to barrier formations [Figure 4b,B]. With the inclusion of C_{methyl}–C_1 relaxation with the other degrees of freedom of the frozen molecule, the variation of ΔV_{ne} with τ again exhibits barrier formation, while both ΔV_{nn} and ΔV_{ee} together contribute to the antibarrier [Figure 4c,C]. Interestingly, with C_{methyl}–H_4 relaxation alone, similar variations of ΔV_{nn}, ΔV_{ee}, and ΔV_{ne} are observed as obtained from C_{methyl}–C_1 relaxation [Figure 4d,D]. The only notable difference is the overall

DOI: 10.1021/acsomega.8b00316
ACS Omega 2018, 3, 6794–6803

Table 1. Principal Bond Energy Changes ($\Delta\omega$) of the $C_{methyl}-C_1$ and $C_{methyl}-H_4$ Bonds Associated with the $-CH_3$ Internal Rotation of the AC Molecule Using MP2/6-21G(d) [B3LYP/6-31G(d,p)] Level of Theory

bond	fully relaxed (kcal/mol)	RR (kcal/mol)	$C_{methyl}-C_1$ and $C_{methyl}-H_4$ relaxed (kcal/mol)	$C_{methyl}-H_5$ and $C_{methyl}-H_6$ relaxed (kcal/mol)
$C_{methyl}-C_1$	7.4 [6.92]	1.25 [1.15]	7.39 [6.88]	−0.52 [−0.39]
$C_{methyl}-H_4$	7.2 [6.49]	1.12 [1.06]	7.16 [6.39]	−0.32 [−0.28]

decrease in the barrier-forming energy associated with ΔV_{ne}. However, combinations of both $C_{methyl}-C_1$ and $C_{methyl}-H_4$ bonds relaxation faithfully reproduce the energy profile for the fully relaxed rotations [Figure 4e,E and a,A]. These results thus indicate that both $C_{methyl}-C_1$ skeletal flexing together with the in-plane $C_{methyl}-H_4$ bond relaxations of the methyl group of the AC molecule play a crucial role toward the genesis of the internal rotational barrier of the AC molecule. The observation is not surprising; the initial inklings were reflected from the variations of NVs, which presage the co-existence of both $C_{methyl}-C_1$ and $C_{methyl}-H_4$ bond relaxations to be the cause of strain within the AC molecule as it undergoes conformational changes from "E" to "S" configurations (vide supra). Apart from understanding the origin behind the rotational barrier of the molecule, the observations from the variations of NVs and the dissected energies further reveal the multidimensional character of the hindered potential. The hindered potential is thus not only an explicit function of τ, but it is strongly coupled with the flexing of $C_{methyl}-C_1$ and $C_{methyl}-H_4$ bonds of the AC molecule.

The coupling of $C_{methyl}-C_1$ and $C_{methyl}-H_4$ bonds with the torsion angle τ of the AC molecule is further reflected from the algebraic sign of the "V_6" value. It is shown in Table S2. The negative sign of "V_6" for the AC molecule, in the case of fully relaxed rotation, turns to a positive sign when both $C_{methyl}-C_1$ and $C_{methyl}-H_4$ relaxations are frozen simultaneously. The abovementioned coupling results in large variations of the in-plane bending $C_1-C_{methyl}-H_4$ angle (associated with $C_{methyl}-C_1$ and $C_{methyl}-H_4$ bond relaxations) with τ, as shown in Figure S2a, further corroborate the abovementioned conjecture. Interestingly, the associated angles with other degrees of freedom of the AC molecule (ca. $C_1-C_{methyl}-H_5$, $C_1-C_{methyl}-H_6$, and $C_{methyl}-C_1-Cl_3$) do not undergo significant variations with τ as depicted in Figure S2b–d. These results substantiate weak involvement of $C_1-C_{methyl}-H_5$, $C_1-C_{methyl}-H_6$, and $C_{methyl}-C_1-Cl_3$ angles toward the origin of the barrier due to the internal rotation of the AC molecule.

The coupling matrix (H_{12}) element for the $C_{methyl}-H_4$ relaxation has been envisaged using the relation[28]

$$\Delta\upsilon = (H_{12})^2/[\upsilon_{torsion} - \upsilon_{\beta(C_{methyl}-H_4)}] \quad (8)$$

The H_{12} has been estimated to be 74.73 and 78.58 cm^{-1} as obtained from DFT and ab initio levels of theories, respectively. The large value of H_{12} suggests strong coupling between torsion and in-plane $\beta(C_{methyl}-H_4)$ bending of the AC molecule.

Thus, unlike acetaldehyde, the reason behind the rotational barrier for the AC molecule is mainly owing to the flexing of in-plane $C_{methyl}-C_1$ and $C_{methyl}-H_4$ bond relaxations, and both of them are coupled with the $-CH_3$ torsional vibration of the molecule. For acetaldehyde, the origin of the barrier is mainly attributed to the in-plane skeletal $C_{methyl}-C_{ald}$ flexing together with the involvement of $-(C_{ald}-H)$ out-of-plane relaxation, involving its aldehyde group. In this connection, it is important to mention that in the AC molecule, the hydrogen atom of the aldehyde 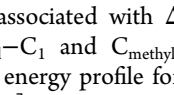 group of the acetaldehyde molecule is replaced by a heavy chlorine atom. The increased inertia of the heavy chlorine atom attached to the 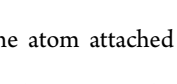 group in the AC molecule is expected to provide impediment toward the relaxation of the C_1-Cl_3 bond. This conjecture is reflected while eliciting the barrier origin of the AC molecule, which involves the skeletal relaxations and the relaxations of the $C_{methyl}-H_4$ bond only, involving the rotor $-CH_3$ group of the molecule. The weak involvement of H_5 and H_6 atoms to the potential energy barrier of the AC molecule may be rationalized from the electronic effect. The inclusion of the out-of-plane $C_{methyl}-H$ skeletal flexing (involving both $C_{methyl}-H_5$ and $C_{methyl}-H_6$ bonds) and the variation of NV as a function of torsion angle (τ) show an antagonistic behavior with respect to RR [Figure 3]. Moreover, we checked the calculations and estimated the variations of potential energy differences for ΔV_{nn}, ΔV_{ee}, and ΔV_{ne} as a function of "τ". The out-of-plane $C_{methyl}-H$ relaxations, involving H_5 and H_6 atoms, do not reproduce the energy profile for the fully relaxed rotation. They are shown in Figure S3. Both these observations signify that H_5 and H_6 are not relevant to the potential energy barrier of the AC molecule.

The electronic structure of the AC molecule in terms of natural bond orbitals (NBOs) primarily comprises three C−H, one C−C, one C−Cl, and two C−O (one σ and one π) bonds, together with two and three localized lone-pair electrons on the oxygen and chlorine atoms, respectively. Bonding and the lone-pair NBOs contribute to 99.1, 99.11% of the electronic charge in the E, S forms of the AC molecule. To understand the weak involvement of H_5 and H_6 atoms to the potential energy barrier of the AC molecule from the electronic effect, the principal bond energy changes ($\Delta\omega$) associated with the internal rotations of the $-CH_3$ group of the molecule have been considered. Accordingly

$$\Delta\omega = \varepsilon_T\rho_T - \varepsilon_B\rho_B \quad (9)$$

where ε_T, ρ_T and ε_B, ρ_B are the NBO energies, electron occupancies corresponding to the staggered (S) and eclipsed (E) forms of the AC molecule, respectively.[11b,12] The bond energy changes associated with the $-CH_3$ group of the molecule are shown in Table 1. From Table 1, it has been observed that for fully relaxed rotation, the barrier-forming terms for the $-CH_3$ group of the AC molecule arises from $C_{methyl}-C_1$ and $C_{methyl}-H_4$ bonds. Significant bond energy changes ($\Delta\omega$) have been noted for $C_{methyl}-C_1$ and $C_{methyl}-H_4$ bonds in the case of RRs with respect to fully relaxed ones. Interestingly, when $C_{methyl}-C_1$ together with $C_{methyl}-H_4$ bonds are allowed to relax, the change in bond energies ($\Delta\omega$) of the $C_{methyl}-C_1$ and $C_{methyl}-H_4$ bonds closely mimic the energies as obtained for fully relaxed rotation. These results further corroborate our earlier conjecture which presages the involvement of both $C_{methyl}-C_1$ skeletal flexing along with the in-plane relaxations of $C_{methyl}-H_4$ bond toward the origin of

DOI: 10.1021/acsomega.8b00316
ACS Omega 2018, 3, 6794−6803

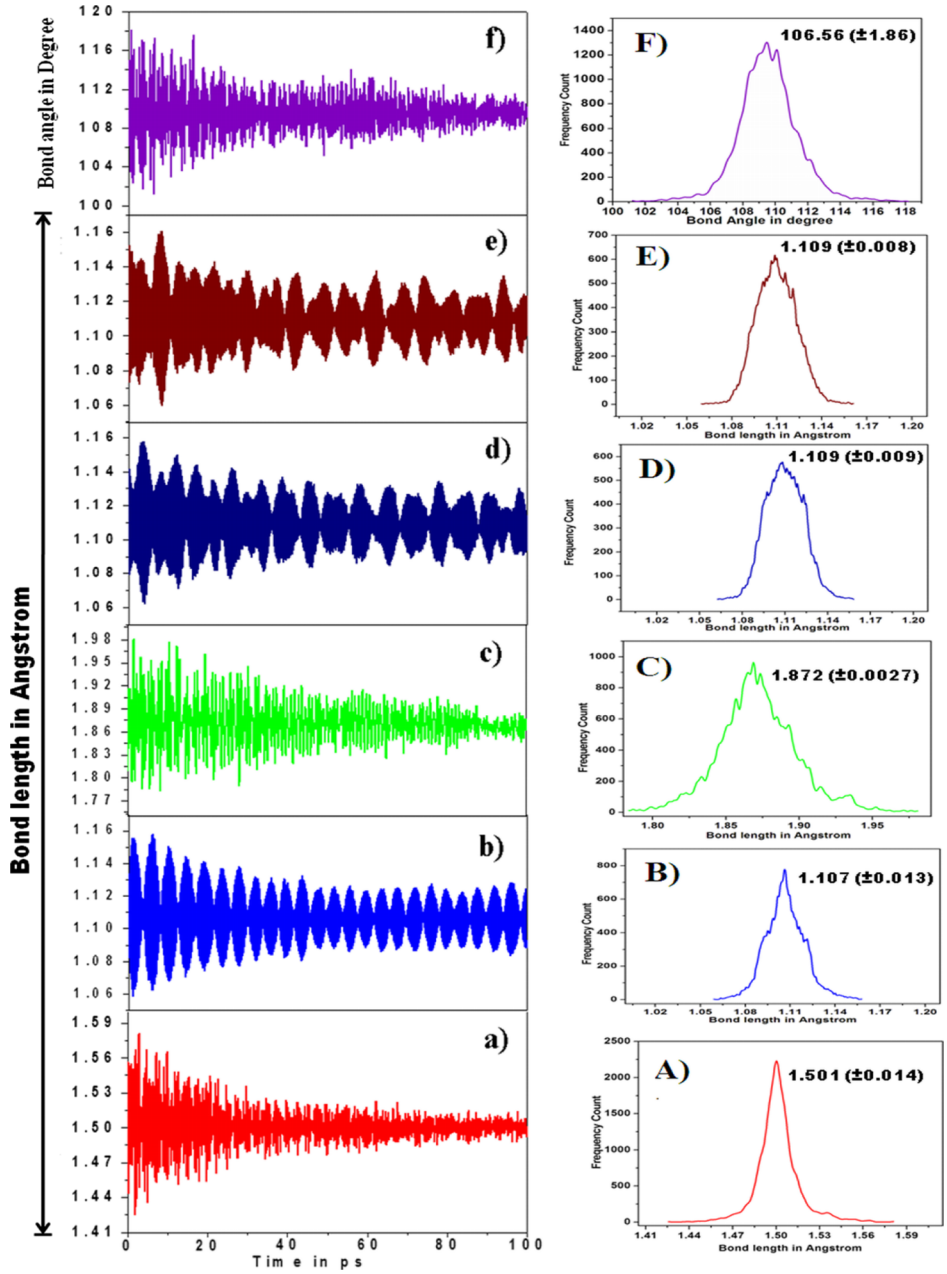

Figure 5. Time evolution and the corresponding frequency counts of (a,A) C_{methyl}–C_1, (b,B) C_{methyl}–H_4, (c,C) C_1–Cl_3, (d,D) C_{methyl}–H_5, (e,E) C_{methyl}–H_6 bond lengths, and (f,F) C_1–C_{methyl}–H_4 bond angle of the AC molecule as obtained from the CPMD calculations.

the barrier due to the internal rotation of the AC molecule (vide ante). However, the effect of combined relaxations of C_{methyl}–H_5 and C_{methyl}–H_6 shows not only small changes in bond energies for the C_{methyl}–C_1 and C_{methyl}–H_4 bonds but exhibits antagonistic behavior with respect to the fully relaxed rotation. The abovementioned results thus signify that involvements of H_5 and H_6 atoms are very weak and are not relevant to the potential energy barrier of the AC molecule.

To introspect an in-depth analysis leading to the origin of the barrier of the AC molecule, the evolution of C_{methyl}–C_1, C_{methyl}–H_4, C_{methyl}–H_5, C_{methyl}–H_6, C_1–Cl_3 bond lengths, and C_1–C_{methyl}–H_4 bond angles with time have been estimated from CPMD simulations. The fluctuations of the respective bond lengths and bond angles in the picosecond time scales are shown in the left panel of Figure 5. The corresponding frequency count of the respective C_{methyl}–C_1, C_{methyl}–H_4, C_1–Cl_3, C_{methyl}–H_5, C_{methyl}–H_6 bond lengths, and C_1–C_{methyl}–H_4 bond angles are also shown in the right panel of Figure 5. The inset of Figure 5A–F shows the respective mean values and the standard deviations (SD) of bond lengths and bond angles with respect to the average peak of the distributions. A closer look of the SD values provides interesting observations. It is clearly seen that the SD values exhibiting fluctuations for in-plane C_{methyl}–C_1 and C_{methyl}–H_4 bond lengths are relatively higher (almost 10 times) in comparison to those for C_1–Cl_3, C_{methyl}–H_5, and C_{methyl}–H_6 bond relaxations. These results further confer the relaxed degrees of freedoms which C_{methyl}–C_1 and C_{methyl}–H_4 bond lengths experience more in comparison to those of C_1–Cl_3, C_{methyl}–H_5, and C_{methyl}–H_6 bonds. The relaxed degrees of freedom for in-plane C_{methyl}–C_1 and C_{methyl}–H_4 bond length flexings are in turn coupled with the torsional vibration of the rotor $-CH_3$ group, resulting in the origin of the

DOI: 10.1021/acsomega.8b00316
ACS Omega 2018, 3, 6794–6803

barrier to the internal rotation of the AC molecule. The involvement of the in-plane relaxation of the $C_{methyl}-H_4$ bond results in the variation of the associated angle $C_1-C_{methyl}-H_4$ which also exhibits a considerable SD value with respect to the equilibrium bond angle of the molecule, settled at ∼106.56° [Figure 5].

The VDOS of the $C_{methyl}-C_1$ and $C_{methyl}-Cl_3$ stretching modes have been mapped in the configuration space from wavelet transform and are shown in Figure 6b,c, respectively.

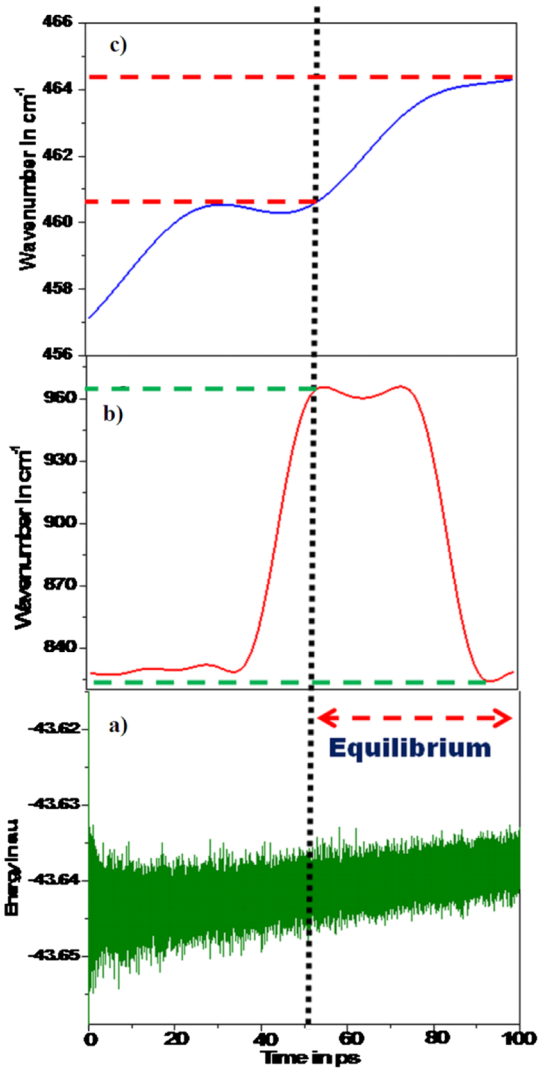

Figure 6. (a) Energy vs time plot for the AC molecule as obtained from CPMD simulation. Time-resolved band stretching frequencies of (b) $C_{methyl}-C_1$ and (c) C_1-Cl_3 bonds of the AC molecule as obtained from wavelet transformation analysis.

Prior to that, the energy of the system has been allowed to equilibrate over 0−100 ps to approximately identify the time scale from where the system accomplishes equilibrium configuration. The corresponding energy versus time plot is shown in Figure 6a. The time coordinate is marked with the vertical dotted line, beyond which the system remains in equilibrium. It is clearly seen from Figure 6b,c that under equilibrium conditions, the vibrational stretching frequencies of $\nu(C_{methyl}-C_1)$ and $\nu(C_{methyl}-Cl_3)$ vary between ∼823 to 960 and 460−464 cm^{-1}, respectively. These results again signify that the flexing of the $C_{methyl}-C_1$ bond is quite large in comparison to $C_{methyl}-Cl_3$.

3.1. Understanding the Origin behind the Barrier from NBO Analyses. As the attractive component of potential energy ΔV_{ne} turns out to be the prominent barrier-forming term for the AC molecule (vide ante), the hyperconjugative or the delocalization energy changes (ΔE_{deloc}) due to rotations of the $-CH_3$ group of the AC molecule have been estimated. The change in attractive potential energy ΔV_{ne} can be linked with the transfer of electrons per se as the hyperconjugative or delocalization (ΔE_{deloc}) energy changes.[10b] The NBO analyses involve the estimations of all possible interactions between "filled" (donor) Lewis type NBOs and "empty" (acceptor) non-Lewis NBOs, by considering their energetic importance using second-order perturbation theory.[30,31] For each donor NBO (i) and acceptor (j), the stabilization energy $\Delta E_{ij}^{(2)}$ associated with delocalization $i \rightarrow j$ is represented as

$$\Delta E_{ij}^{(2)} = \frac{|\langle \psi_i | \hat{F} | \psi_j \rangle|^2}{\varepsilon_j - \varepsilon_i} \quad (10)$$

where $\hat{F}$ is the Fock operator, and ϵ_i and ϵ_j correspond to the energy eigen states of $|\psi_i\rangle$ and $|\psi_j\rangle$ molecular orbitals, respectively.

The principal bond−antibond interaction energies related to the internal rotational barrier between "E" and "S" forms of the AC molecule are shown in Table 2. The prominent barrier-forming energy is noted for $C_{methyl}-H_4(\sigma)/C1-Cl_3(\sigma)^*$ interactions, undergoing significant change in stabilization energy $\Delta E_{ij}^{(2)}$ = ≈ 3.32 kcal/mol. The 2D-contour plots of the orbitals involved in bond−antibond $C_{methyl}-H_4(\sigma)/C1-Cl_3(\sigma)^*$ interactions for "E" and "S" forms of the AC molecule, as obtained from DFT calculation is shown in Figure 7. From Figure 7, it is seen that the $C_{methyl}-H_4(\sigma)$ bonding and the $C_1-Cl_3(\sigma)^*$ antibonding orbitals show a favorable overlap in the region of the $C_{methyl}-C_1$ bond for the "E" form ($F_{i,j}$ = 0.056 au)

Table 2. Principal Barrier-Forming Bond−Antibond and Lone Pair−Antibond Interactions (in kcal/mol) for the $-CH_3$ Rotational Barrier of the AC Molecule Using B3LYP/6-31G(d,p) [MP2/6-21G(d)] Level of Theory

bond−antibond interaction (donor/acceptor)	$E_{ij}^{(2)}$ (kcal/mol)
$C_{methyl}-H_4(\sigma)/C1-Cl_3(\sigma)^*$	3.32 [3.56]
LP $O_2/C_1-Cl_3(\sigma)^*$	0.76 [0.89]
$C_4-H_6(\sigma)/C_1-O_2(\sigma)^*$	0.62 [0.67]

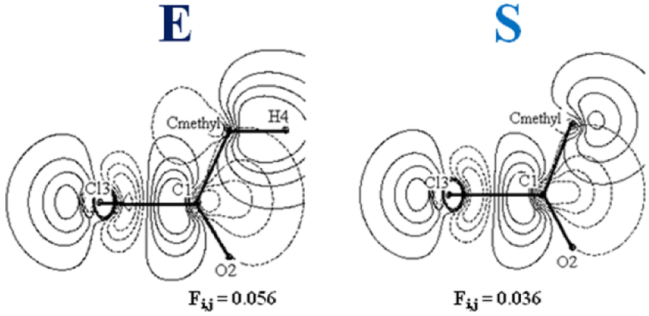

Figure 7. Orbital contour diagram for $C_{methyl}-H_4(\sigma)$ bonding and $C_1-Cl_3(\sigma)^*$ antibonding pre-NBO in "E" and "S" forms of the AC molecule using the B3LYP/6-31G(d,p) level of theory.

DOI: 10.1021/acsomega.8b00316
ACS Omega 2018, 3, 6794−6803

of the AC molecule leading to the charge transfer interactions from the methyl group to the C_1-Cl_3 fragment of the molecule. The same orbital, for the "S" conformer of the AC molecule, however, exhibits a relatively weak overlap ($F_{i,j}$ = 0.036 au) in the region of the abovementioned σ bond. The above-mentioned result signifies that the flexing of the $C_{methyl}-C_1$ bond may thus be explained by considering favorable $C_{methyl}-H_4(\sigma)/C_1-Cl_3(\sigma)^*$ bonding and antibonding overlap around the $C_{methyl}-C_1$ bond region for the "E" conformer in comparison to that of its "S" form associated with the methyl internal rotation of the AC molecule. Thus, the effect of hyperconjugation associated with $C_{methyl}-H_4(\sigma)/C_1-Cl_3(\sigma)^*$ bond−antibond interactions plays an effective role toward the relaxations of both $C_{methyl}-C_1$ and $C_{methyl}-H_4$ bonds which in turn coupled with the methyl torsion and contribute toward the origin of barrier due to the internal rotation of the AC molecule.

4. CONCLUSIONS

The origin of the rotational barrier for the AC molecule has been explored for the first time from the NV, relaxation effects, and natural bond orbital (NBO) analysis techniques. The NVs, dissection of energies, and NBO analyses all confirm the multidimensional character of the hindered potential of the concerned molecule. The hindered potential is found not only to be an explicit function of torsional angle (τ) but is strongly coupled with the flexing of $C_{methyl}-C_1$ and $C_{methyl}-H_4$ bonds of the molecule. The available experimental results for the AC molecule further encourage us to harmonize the experimentally estimated 3-fold rotational barrier (V_3) of the molecule with the theoretically predicted result. The large negative value of "V_6" signifies coupling of $C_{methyl}-C_1$ and $C_{methyl}-H_4$ bond relaxations with the $-CH_3$ torsional vibration of the molecule. The coupling matrix (H_{12}) element as obtained from DFT and ab initio levels of theories both substantiate the above-mentioned conjecture. Substitution of a heavy chlorine atom and its restricted motion is reflected from the time-resolved band stretching frequency of the C_1-Cl_3 bond of the AC molecule, as obtained from wavelet transformation analyses. Theoretical methodologies finally reveal that the relaxations of both the in-plane $C_{methyl}-C_1$ and $C_{methyl}-H_4$ bonds together play a significant role toward understanding the barrier to internal rotation for the AC molecule.

■ ASSOCIATED CONTENT

Supporting Information

The Supporting Information is available free of charge on the ACS Publications website at DOI: 10.1021/acsomega.8b00316.

PEC as a function of torsion angle (τ) about the $C_{methyl}-C_1$ bond of the $-CH_3$ group of the AC molecule as obtained from (a) B3LYP/6-31G(d,p) and (b) MP2/6-21G(d) level of theories; relevant structural parameters (bond length in Å, bond angles in degrees) of "E" and "S" forms of the AC molecule calculated at MP2/6-21G(d), B3LYP/6-31G(d,p), and CPMD level of theories; theoretically fitted "V_3" and "V_6" coefficients for the methyl rotational barrier of the AC molecule using B3LYP/6-31G(d,p) [MP2/6-21G*] level of theory; variation of the (a) $C_1-C_{methyl}-H_4$, (b) $C_1-C_{methyl}-H_4$, (c) $C_1-C_{methyl}-H_6$, and (d) $C_{methyl}-C_1-Cl_3$ angles of the AC molecule with torsion angle (τ) as obtained from B3LYP/6-31G(d,p) level of theory; and rotational dependence of ΔV_{nn}, ΔV_{ee}, and ΔV_{ne} of the (a,A) out-of-plane $C_{methyl}-H_5$ and (b,B) out-of-plane $C_{methyl}-H_6$ skeletal flexing of the AC molecule (PDF)

■ AUTHOR INFORMATION

Corresponding Author

*E-mail: joydeep72_c@rediffmail.com. Phone: (033)24138917 (J.C.).

ORCID

Joydeep Chowdhury: 0000-0001-9952-9956

Notes

The authors declare no competing financial interest.

■ ACKNOWLEDGMENTS

Authors express their thanks to the Department of Science and Technology (DST) and Department of Atomic Energy (DAE-BRNS), India, for the financial support through the research projects (project nos. SR/S2/CMP-0045/2012; 2012/37P/BRNS). Authors also like to thank the Department of Physics, Jadavpur University, for providing departmental computational facility through the DST-FIST programme.

■ REFERENCES

(1) (a) Gao, Y.; Zhou, Y.; Goldstein, J. L.; Brown, M. S.; Radhakrishnan, A. Cholesterol-induced conformation changes in the sterol-sensing domain of the scap protein suggest feedback mechanism to control cholesterol synthesis. *J. Biol. Chem.* **2017**, *292*, 8729−8737. (b) Giliberti, V.; Badioli, M.; Nucara, A.; Calvani, P.; Ritter, E.; Puskar, L.; Aziz, E. F.; Hegemann, P.; Schade, U.; Ortolani, M.; Baldassarre, L. Heterogeneity of the Transmembrane Protein Conformation in Purple Membranes Identified by Infrared Nanospectroscopy. *Small* **2017**, *13*, 1701181. (c) Sánchez-Rico, C.; von Voithenberg, L. V.; Warner, L.; Lamb, D. C.; Sattler, M. Effects of Fluorophore Attachment on Protein Conformation and Dynamics Studied by spFRET and NMR Spectroscopy. *Chem.—Eur. J.* **2017**, *23*, 14267−14277.

(2) (a) Mizushima, S.-i.; Morino, Y.; Takeda, M. Molecular Configurations in Rotational Isomerism. *J. Chem. Phys.* **1941**, *9*, 826. (b) Mizushima, S.-i.; Morino, Y.; Watanabe, I.; Simanouti, T.; Yamaguchi, S. Raman Effect, Infra-Red Absorption, Dielectric Constant, and Electron Diffraction in Relation to Internal Rotation. *J. Chem. Phys.* **1949**, *17*, 591−594.

(3) Nielsen, H. H. The Torsion Oscillator-Rotator in the Quantum Mechanics. *Phys. Rev.* **1932**, *40*, 445−456.

(4) Pitzer, K. S. Thermodynamics of Gaseous Hydrocarbons: Ethane, Ethylene, Propane, Propylene, n-Butane, Isobutane, 1-Butene, Cis and Trans 2-Butenes, Isobutene, and Neopentane (Tetramethylmethane). *J. Chem. Phys.* **1937**, *5*, 473−479.

(5) Gordy, W.; Cook, R. L. *Microwave Molecular Spectra*; John Wiley & Sons, 1984; pp 477−479.

(6) (a) Durig, J. R.; Wang, A. Y.; Little, T. S. Conformational stability, barriers to internal rotation, vibrational assignment, and ab initio calculations of 2-chloropropenoyl fluoride. *J. Chem. Phys.* **1990**, *93*, 905−917. (b) Durig, J. R.; Bergana, M. M.; Phan, H. V. Raman and infrared spectra, conformational stability, barriers to internal rotation, ab initio calculations and vibrational assignment of dichloroacetyl fluoride. *J. Raman Spectrosc.* **1991**, *22*, 141−154. (c) Durig, J. R.; Guirgis, G. A.; Phan, H. V. Far-infrared spectrum, conformational stability, barriers to internal rotation, ab initio calculations, and vibrational assignment of propionyl bromide. *J. Mol. Struct.* **1991**, *244*, 139−164. (d) Durig, J. R.; Kenton, R.; Phan, H. V.; Little, T. S. Far-infrared spectra and barriers to internal rotation of pivaldehyde, pivaloyl fluoride, pivaloyl chloride and pinacolone. *J. Mol. Struct.* **1991**, *247*, 237−251.

(7) (a) Philis, J. G.; Berman, J. M.; Goodman, L. The acetone a2 torsional vibration. *Chem. Phys. Lett.* **1990**, *167*, 16−20. (b) Gu, H.; Kundu, T.; Goodman, L. Torsional vibrations in jet-cooled

DOI: 10.1021/acsomega.8b00316
ACS Omega 2018, 3, 6794−6803

acetaldehyde. *J. Phys. Chem.* **1993**, *97*, 7194−7200. (c) Kundu, T.; Thakur, S. N.; Goodman, L. Methyl rotor effects on acetone Rydberg spectra. I. The $^1A_2(3p\leftarrow n)\leftarrow{}^1A_1$transition. *J. Chem. Phys.* **1992**, *97*, 5410−5416. (d) Philis, J. G.; Goodman, L. Methyl rotor effects on acetone Rydberg spectra. II. The $^1B_2(3s\leftarrow n)\leftarrow{}^1A_1$transition. *J. Chem. Phys.* **1993**, *98*, 3795−3802.

(8) (a) Naylor, R. E., Jr; Wilson, E. B., Jr Microwave Spectrum and Barrier to Internal Rotation in CH_3BF_2. *J. Chem. Phys.* **1957**, *26*, 1057−1060. (b) Stiefvater, O. L.; Wilson, E. B. Microwave Spectrum, Rotational Isomerism, and Internal Barrier Functions in Propionyl Fluoride. *J. Chem. Phys.* **1969**, *50*, 5385−5403. (c) Beaudet, R. A.; Wilson, E. B., Jr Microwave Spectrum and Barrier to Internal Rotation of cis-1-Fluoropropylene. *J. Chem. Phys.* **1962**, *37*, 1133−1138.

(9) (a) Brunck, T. K.; Weinhold, F. Quantum-mechanical studies on the origin of barriers to internal rotation about single bonds. *J. Am. Chem. Soc.* **1979**, *101*, 1700−1709. (b) Bader, R. F. W.; Cheeseman, J. R.; Laidig, K. E.; Wiberg, K. B.; Breneman, C. Origin of rotation and inversion barriers. *J. Am. Chem. Soc.* **1990**, *112*, 6530−6536. (c) Hehre, W. J.; Pople, J. A.; Devaquet, A. J. P. Torsional potentials of methyl rotors attached to polar linkages. *J. Am. Chem. Soc.* **1976**, *98*, 664−668. (d) Radom, L.; Baker, J.; Gill, P. M. W.; Nobes, R. H.; Riggs, N. W. A theoretical approach to molecular conformational analysis. *J. Mol. Struct.* **1985**, *126*, 271−290. (e) Pross, A.; Radom, L.; Riggs, N. V. A theoretical approach to substituent effects. Structural consequences of methyl hyperconjugation. Methyl tilt angles and carbon-hydrogen bond lengths. *J. Am. Chem. Soc.* **1980**, *102*, 2253−2259.

(10) (a) Goodman, L.; Gu, H.; Pophristic, V. Gauche Effect in 1,2-Difluoroethane. Hyperconjugation, Bent Bonds, Steric Repulsion. *J. Phys. Chem. A* **2005**, *109*, 1223−1229. (b) Pophristic, V.; Goodman, L. Hyperconjugation not steric repulsion leads to the staggered structure of ethane. *Nature* **2001**, *411*, 565−568. (c) Pophristic, V.; Goodman, L.; Gorb, L.; Leszczynski, J. Acetone n-radical cation conformational preference and torsional barrier. *J. Chem. Phys.* **2002**, *116*, 7049−7056. (d) Goodman, L.; Pophristic, V. *The Encyclopedia of Computational Chemistry*; John Wiley and Sons, 1998; Vol. *IV*, pp 2577−2598.

(11) (a) Dutta, B.; De, R.; Pal, C.; Chowdhury, J. Vibrational analysis of the conformers and understanding the genesis of the internal rotational barriers of Isobutyl Cyanide molecule. *Spectrochim. Acta, Part A* **2012**, *96*, 837−847. (b) Dutta, B.; Chowdhury, J. Origins of threefold rotational barriers of molecule containing two methyl groups: Ethyl propionate as paradigm. *Chem. Phys. Lett.* **2014**, *612*, 89−96.

(12) Guo, D.; Goodman, L. Nature of Barrier Forces in Acetaldehyde. *J. Phys. Chem.* **1996**, *100*, 12540−12545.

(13) Durig, J. R.; Davis, J. F.; Guirgis, G. A. Raman and far infrared spectra, structural parameters, and ab initio calculations on acetyl chloride. *J. Raman Spectrosc.* **1994**, *25*, 189−198.

(14) (a) Grove, E. L.; Perkins, A. J. *Developments in Applied Spectroscopy*; Springer Science & Business Media, Dec 06, 2012; Vol *9*. (b) Sinnott, K. M. Microwave Spectrum of Acetyl chloride. *J. Chem. Phys.* **1961**, *34*, 851−861.

(15) Frisch, M. J.; Trucks, G. W.; Schiegel, H. B.; Scuseria, G. E.; Robb, M. A.; Cheeseman, J. R.; Montgomery, J. A.; Vreven, T., Jr; Kudin, K. N.; Burant, J. C.; et al. *Gaussian 09*; Gaussian, Inc.: Pittsburgh, PA, 2009.

(16) Moule, D. C.; Smeyers, Y. G.; Senent, M. L.; Clouthier, D. J.; Karolczak, J.; Judge, R. H. An analysis of the methyl rotation dynamics in the S_0 (X^1A_1) and T_1 (a^3A_2) states of thioacetone, $(CH_3)_2CS$ and $(CD_3)_2CS$ from pyrolysis jet spectra. *J. Chem. Phys.* **1991**, *95*, 3137−3146.

(17) CPMD. http://www.cpmd.org/, Copyright IBM Corp 1990-2008, Copyright MPI fur Festkorperforschung Stuttgart 1997−2001.

(18) Marx, D.; Hutter, J. *Modern Methods and Algorithms of Quantum Chemistry*; NIC Series; Forschungszentrum Julich, 2000; pp 301−449.

(19) (a) Nosé, S. A unified formulation of the constant temperature molecular dynamics methods. *J. Chem. Phys.* **1984**, *81*, 511−519. (b) Hoover, W. G. Canonical dynamics: Equilibrium phase-space distributions. *Phys. Rev. A: At., Mol., Opt. Phys.* **1985**, *31*, 1695−1697.

(20) Perdew, J. P.; Burke, S.; Ernzerhof, M. Generalized Gradient Approximation Made Simple. *Phys. Rev. Lett.* **1996**, *77*, 3865−3868.

(21) Troullier, N.; Martins, J. L. Efficient pseudopotentials for plane-wave calculations. *Phys. Rev. B: Condens. Matter Mater. Phys.* **1991**, *43*, 1993−2006.

(22) Pagliai, M.; Muniz-Miranda, F.; Cardini, G.; Righini, R.; Schettino, V. Hydrogen Bond Dynamics of Methyl Acetate in Methanol. *J. Phys. Chem. Lett.* **2010**, *1*, 2951.

(23) Muniz-Miranda, M.; Pagliai, M.; Muniz-Miranda, F.; Schettino, V. Raman and computational study of solvation and chemisorption of thiazole in silver hydrosol. *Chem. Commun.* **2011**, *47*, 3138−3140.

(24) Kirby, J. F.; Swain, C. J. Power spectral estimates using two-dimensional Morlet-fan wavelets with emphasis on the long wavelengths: jackknife errors, bandwidth resolution and orthogonality properties. *Geophys. J. Int.* **2013**, *194*, 78−99.

(25) (a) Polavarapu, P. L. Ab initio vibrational Raman and Raman optical activity spectra. *J. Phys. Chem.* **1990**, *94*, 8106−8112. (b) Chantry, G. W. *The Raman Effect*; Anderson, A., Eds.; Marcel Dekker: New York, 1971; Vol. *1*, p 49. (c) Dekker, M. *The Raman Effect*; Marcel Dekker: New York, 1971; Vol. *1*, Chapter 2.

(26) Brela, M. Z.; Wójcik, M. J.; Boczar, M.; Witek, Ł.; Yasuda, M.; Ozaki, Y. Car−Parrinello Molecular Dynamics Simulations of Infrared Spectra of Crystalline Vitamin C with Analysis of Double Minimum Proton Potentials for Medium-Strong Hydrogen Bonds. *J. Phys. Chem. B* **2015**, *119*, 7922−7930.

(27) Kudich, A. V.; Bataev, V. A.; Godunov, I. A. Structure of acetyl chloride molecule isotopomers CH3COCl and CD3COCl in the ground and lowest excited singlet and triplet electronic states: a quantum mechanical study. *Russ. Chem. Bull.* **2005**, *54*, 62−70.

(28) Goodman, L.; Leszczynski, J.; Kundu, T. Sign of V_6 term in internal rotation potential of acetaldehyde. Theory and experiment in harmony. *J. Chem. Phys.* **1994**, *100*, 1274.

(29) (a) Moule, D. C.; Smeyers, Y. G.; Senent, M. L.; Clouthier, D. J.; Karolczak, J.; Judge, R. H. An analysis of the methyl rotation dynamics in the S_0 (X^1A_1) and T_1 (a^3A_2) states of thioacetone, $(CH_3)_2CS$ and $(CD_3)_2CS$ from pyrolysis jet spectra. *J. Chem. Phys.* **1991**, *95*, 3137−3146. (b) Wilson, E. B. Four-dimensional electron density function. *J. Chem. Phys.* **1962**, *36*, 2232−2233. (c) Politzer, P.; Parr, R. G. Some new energy formulas for atoms and molecules. *J. Chem. Phys.* **1974**, *61*, 4258−4262. (d) Matta, C. F.; Sadjadi, S. A.; Braden, D. A.; Frenking, G. The barrier to the methyl rotation in cis-2-butene and its isomerization energy to trans-2-butene revisited. *J. Comput. Chem.* **2016**, *37*, 143−154.

(30) Goodman, L.; Gu, H. Flexing analysis of steric exchange repulsion accompanying ethane internal rotation. *J. Chem. Phys.* **1998**, *109*, 72−78.

(31) Reed, A. E.; Weinhold, F. Natural Bond Orbital Analysis of Internal Rotation Barriers and Related Phenomena. *Isr. J. Chem.* **1991**, *31*, 277−285.

DOI: 10.1021/acsomega.8b00316
ACS Omega 2018, 3, 6794−6803